Effective time-dependent temperature for fermionic master equations beyond the Markov and the secular approximations

Lukas Litzba [1,*] Eric Kleinherbers [1,2,†] Jürgen König [1] Ralf Schützhold,[3,4] and Nikodem Szpak [1,‡]

[1]*Fakultät für Physik and CENIDE, Universität Duisburg-Essen, Lotharstraße 1, Duisburg 47057, Germany*

[2]*Department of Physics and Astronomy, University of California, Los Angeles, California 90095, USA*

[3]*Helmholtz-Zentrum Dresden-Rossendorf, Bautzner Landstraße 400, 01328 Dresden, Germany*

[4]*Institut für Theoretische Physik, Technische Universität Dresden, 01062 Dresden, Germany*

(Received 30 July 2024; revised 20 December 2024; accepted 13 January 2025; published 3 February 2025)

We consider a fermionic quantum system exchanging particles with an environment at a fixed temperature and study its reduced evolution by means of a Redfield-I equation with time-dependent (non-Markovian) coefficients. We find that the description can be efficiently reduced to a standard-form Redfield-II equation, however, with a *time-dependent effective bath temperature* obeying a universal law. At early times, after the system and environment start in a product state, the *effective temperature* appears to be very high, yet eventually it settles down towards the true environment value. In this way, we obtain a time-local master equation, offering high accuracy at all times and preserving the crucial properties of the density matrix. It includes non-Markovian relaxation processes beyond the secular approximation and time-averaging methods and can be further applied to various types of Gorini-Kossakowski-Sudarshan-Lindblad equations. We derive the theory from first principles and discuss its application using a simple example of a single quantum dot.

DOI: 10.1103/PhysRevB.111.085103

I. INTRODUCTION

When dealing with open quantum systems [1] interacting with an infinite environment, exact solutions can be found in some special cases [2–11]. However, as soon as any interactions, such as Coulomb, are present it becomes almost impossible to solve them exactly [2,12–14]. In order to explore the system alone, it is possible to eliminate the baths from the description and obtain a formally exact time-nonlocal (non-Markovian) master equation [15–20] for the quantum system which contains information about the full history including the formation of coherences between the environment and the system [1,6].

At the lowest order of perturbation theory in the system-bath coupling, using the (first) Markov assumption, it can be approximated by the time-local master equation for the system's density matrix with time-dependent (non-Markovian) coefficients, known as the Redfield-I equation [1,21]. It does not include the history of the system and of the bath but its time-dependent coefficients maintain residual information about the formation of coherences between the environment and the system. The latter is related to non-Markovian effects present also in unstructured environments (e.g., such as the wide-band limit) which are usually treated as Markovian. Although the Redfield-I equation offers a good approximation of the system dynamics [22] it is also known for its mathematical problems, originating in the first-order time-dependent perturbation theory, of not preserving the positivity of the density matrix which may result in negative probabilities and nonphysical behavior of observables [22–27].

Partially these problems are related to the transition rates of the system described by the time-dependent coefficients, which we denote symbolically $F_{\Delta E,T_B}(t)$ (for transition energy ΔE and temperature T_B), showing excessive oscillations and becoming temporarily negative (problem 1). In order to remove the oscillations, an additional approximation extends the initial integration time to the infinite past ($t_0 \to -\infty$) by which the resulting Liouville operator becomes time independent and gives the (now Markovian) Redfield-II master equation with static and positive coefficients $F_{\Delta E,T_B}(\infty)$. Those, however, show another problem (the more popular one of the two, regarding literature): not only single coefficients $F_{\Delta E,T_B}$ but also their (matrix-valued) combinations, involved in generic transitions with different transition energies ΔE, can lead to excess coherences between energy states and thus also violate the positivity of the density matrix (problem 2) [22–27].

A standard, however drastic, way to deal with the latter problem is the secular approximation [1,28] that artificially removes energy coherences from the system by which the master equation attains the Gorini-Kossakowski-Sudarshan-Lindblad (GKSL) form which preserves all important properties of the density matrix [1,29–31]. However, the secular approximation is known to miss some important physical information about coherences between energy states in the

*Contact author: lukas.litzba@uni-due.de

†Contact author: ekleinherbers@physics.ucla.edu

‡Contact author: nikodem.szpak@uni-due.de

system, as demonstrated, e.g., in [26,27,32–34]. Along similar lines as in [35–38], in [26,34] we proposed a refined method of *coherent approximation* which allows to keep the mathematically maximal amount of coherences in the system, also leading to a GKSL equation. In addition, there exist further regularization methods [37,39–42] which also lead to GKSL master equations. Due to their simplicity and direct interpretation of the jump operators, the GKSL master equations can be usually derived from phenomenological [26,36] or microscopic [22,26,37,39,40] points of view.

However, due to their Markovian behavior, the GKSL equations neglect memory effects and relaxation dynamics of the environment as well as effects related to the formation of coherences between the environment and the system. In particular, neglecting the time dependence of the coefficients leads to a loss of accuracy at short times which can be partly compensated by the "initial slip" method, artificially adjusting the initial state of the system to the later development [24,25,43]. The behavior at short times has been also discussed in the context of time-local master equations [37,40,44–46]. One popular approach which deals with the problem of time-dependent coefficients is the dynamical coarse graining (DCG) method [44]. It improves the behavior at short times and preserves the properties of the density matrix. However, due to the averaging character of the coarse graining, this method becomes similar to the secular approximation for late times, affected by the above-mentioned problems.

In Ref. [22], various master equations have been compared with exact solutions. The general conclusion was that "the simple Redfield-I equation with time-dependent coefficients is significantly more accurate than all other methods." Therefore, we take it as a natural starting point to study a generic tunnel coupling between the system and a fermionic environment. Studying the time-dependent coefficients $F_{\Delta E,T_\mathrm{B}}(t)$ in more detail, we realized that their defining integrals, parametrized by the time t, temperature T_B, and energy difference ΔE, can be very accurately and uniformly in all three parameters approximated by a simple family of functions $\mathcal{F}_{\Delta E,T_\mathrm{B}}(t)$, obtained by approximate calculation of their defining integral. A surprising observation is that the result has again the form of the static coefficients $F_{\Delta E,T(t)}(\infty)$ with now time-dependent temperature

$$T(t) = T_\mathrm{B} \Big/ \tanh\left(\frac{4k_\mathrm{B}T_\mathrm{B}}{\hbar\pi}(t-t_0)\right). \tag{1}$$

It is universal in the sense that it depends only on the true bath temperature T_B, the Boltzmann and Planck constants k_B and $\hbar$, the initial time t_0 and time t but not on the energy differences ΔE nor on any details of the system or the coupling. It has the properties that $T(t_0) \to \infty$ and $T(\infty) \to T_\mathrm{B}$. The replacement $T_\mathrm{B} \to T(t)$ leads to a modified Redfield-I equation with time-dependent coefficients, known analytically for all values of parameters ΔE, T_B, and t and satisfying all relevant limiting cases. Most importantly, the time-dependent temperature solves problem 1 since it removes both excessive oscillations and negative values by ensuring $0 \leqslant F_{\Delta E,T(t)}(\infty) \leqslant 1$. It can be naturally combined with the regularization methods, discussed above, to solve problem 2 thus bringing the equation into a time-dependent GKSL form.

The time-dependent temperature $T(t)$ can be interpreted as an effective bath temperature from the perspective of the system. It is conceptually different from time-dependent quasiequilibrium temperatures of the system discussed in [47–50] or time-dependent bath temperatures for finite-size baths discussed in [51–53]. In our case, the time dependence of $T(t)$ is related to the energy gain $[T(t) \geqslant T_\mathrm{B}]$ resulting from the coupling between the system and the bath.

The main goal of this paper is to propose a universal approach in the form of a time-local master equation, offering high accuracy at all times and preserving the properties of the density matrix, which includes non-Markovian relaxation processes beyond the secular approximation and time-averaging methods.

II. MODEL

In the following, we will focus on fermionic systems and fermionic environments which can exchange particles. We consider a finite quantum system described by the Hamiltonian written in its Fock eigenbasis

$$H_S = \sum_{l=1}^{\dim(S)} E_l \, |E_l\rangle \langle E_l| \tag{2}$$

coupled to M fermionic baths, described by the Hamiltonian

$$H_B = \sum_{m=1}^{M} \sum_k \varepsilon_{m,k} \, b_{m,k}^\dagger \, b_{m,k}, \tag{3}$$

via the coupling Hamiltonian

$$H_C = \sum_{m=1}^{M} \sum_k \gamma_{m,k} \, c_m^\dagger \otimes b_{m,k} + \mathrm{H.c.} \tag{4}$$

(brought to the tensor product form via the Jordan-Wigner transformation [54]). Here, $c_m^\dagger$ and c_m are fermionic creation and annihilation operators in the system,[1] respectively, whereas $b_{m,k}^\dagger$ and $b_{m,k}$ are the fermionic creation and annihilation operators, respectively, at bath m in the mode k which are associated with the energy $\varepsilon_{m,k}$ and satisfy $\{b_{m,k}, b_{n,l}^\dagger\} = \delta_{mn}\delta_{kl}$, $\{b_{m,k}, b_{n,l}\} = 0$. The coefficients $\gamma_{m,k}$ give the tunneling amplitudes between the system and the mode k in the bath m. The total Hamiltonian reads then

$$H = H_S \otimes 1_B + 1_S \otimes H_B + H_C. \tag{5}$$

We assume that the dimension of the system, $\dim(S)$, is small compared to the number of degrees of freedom of the baths, $\dim(S) \ll \dim(B)$. This justifies the treatment of the system as open, coupled to the much larger environment, which shall be subsequently eliminated from the description. We assume also that the full system begins its evolution at time $t = t_0$ in a product state described by the density matrix $\rho(t_0) = \rho_S(t_0) \otimes \rho_B(t_0)$ where $\rho_S(t_0)$ refers to the system while

$$\rho_B(t_0) \sim e^{-\left(H_B - \mu \sum_{m,k} b_{m,k}^\dagger b_{m,k}\right)/(k_\mathrm{B}T_\mathrm{B})} \tag{6}$$

refers to the baths at thermal equilibrium (Gibbs state) with temperature T_B and chemical potential μ and satisfies $[H_B, \rho_B] = 0$. For unequal chemical potentials μ_m and

[1]The case where more than one bath, e.g. $m = 1, 2, \ldots, M_1 \leqslant M$, is coupled to the same system mode can be described by the formal substitution $c_1 = c_2 = \ldots = c_{M_1}$.

temperatures $T_{\mathrm{B},m}$, the presented method can be applied analogously giving rise to separate effective temperatures $T_m(t)$ for each bath m.

For a Hamilton operator of the form (5), in Sec. III we will derive a time-dependent Redfield equation including time-dependent coefficients. In Sec. IV, we will discuss these coefficients and identify that their excessive oscillations lead to nonphysical effects. Furthermore, we will demonstrate that the time-dependent coefficients can be interpreted, to a very good approximation, as the static coefficients with a *time-dependent effective temperature* $T(t)$. Using this interpretation, we will find a time-local master equation with positive time-dependent coefficients.

As the simplest example, demonstrating the application of the method, we will consider a single quantum dot with Coulomb interaction coupled to a fermionic bath in which the problems of the time-dependent Redfield-I equation become already apparent. In Sec. V, we will compare the solutions of the Redfield-I equation to its version using the time-dependent temperature and to static GKSL equations. In Sec. VI, we will compare the above approximation schemes with exact solutions obtained for a non-Coulomb-interacting quantum dot.

III. TIME-DEPENDENT REDFIELD EQUATION

In order to effectively eliminate the environment from the description, we apply the Born and the first Markov approximations to the bath and the system evolution and, by tracing out the baths' degrees of freedom in the von Neumann equation expanded to the lowest nonvanishing order in the system-bath couplings, $\mathcal{O}(|\gamma_{m,k}|^2)$, we arrive at the Redfield-I master equation [1,21]

$$\partial_t \rho_{\mathrm{I}}(t) = -\int_0^{t-t_0} \mathrm{d}\tau \; \mathrm{tr}_B[H_{C,I}(t), [H_{C,I}(t-\tau), \rho_{S,I}(t)\otimes\rho_B(t_0)]]. \tag{7}$$

The index "I" indicates the interaction picture with respect to the coupling Hamiltonian H_C. Furthermore, we set $\hbar = 1$ for convenience.

With the baths in thermal equilibrium, satisfying $\langle b^\dagger_{m,k} b_{m',k'}\rangle = \delta_{k,k'}\delta_{m,m'} f_+(\varepsilon_{m,k}, T_{\mathrm{B}})$, and the Fermi function $f_\pm(E, T_{\mathrm{B}}) = [1+\exp\{\pm(E-\mu)/(k_{\mathrm{B}}T_{\mathrm{B}})\}]^{-1}$, the Redfield-I master equation, now in the Schrödinger picture, can be also written in the form

$$\partial_t\, \rho(t) = -i\,[H_S, \rho(t)] + \mathcal{L}_t\, \rho(t) \tag{8}$$

with the superoperator $\mathcal{L}_t$ acting in the full Liouville space which is, in general, not positivity preserving.[2] It can be split into two parts, $\mathcal{L}_t = -i[\delta H_S(t), \cdot] + \widetilde{\mathcal{L}}_t$, of which the first can be included in the "renormalized" (or "Lamb-shifted") Hermitian, possibly time-dependent Hamiltonian

$$\widetilde{H}_S(t) = H_S + \delta H_S(t) = H_S - i \sum_{m,\alpha\Delta E,\Delta E'} \frac{A^\alpha_m(t,\Delta E) - \overline{A^\alpha_m(t,\Delta E')}}{4} \times K^\alpha_m(\Delta E')^\dagger K^\alpha_m(\Delta E) \tag{9}$$

with

$$K^\pm_m(\Delta E) = \sum_{k,l} \delta_{E_k - E_l, \pm\Delta E} |E_k\rangle\langle E_k| c^\pm_m |E_l\rangle\langle E_l| \tag{10}$$

and

$$A^\pm_m(t,\Delta E) = 2\int_0^{t-t_0} \mathrm{d}\tau \sum_k |\gamma_{m,k}|^2 f_\pm(\varepsilon_{m,k}, T_{\mathrm{B}})\, e^{\pm i(\varepsilon_{m,k}-\Delta E)\tau} = \int_0^{t-t_0} \mathrm{d}\tau \int_{-\infty}^{\infty} \frac{\mathrm{d}\omega}{\pi} \Gamma_m(\omega) f_\pm(\omega, T_{\mathrm{B}})\, e^{\pm i(\omega-\Delta E)\tau}, \tag{11}$$

where we introduced $c^-_m = c_m$, $c^+_m = c^\dagger_m$, and $\Gamma_m(\omega) = 2\pi\sum_k |\gamma_{m,k}|^2 \delta(\omega - \varepsilon_{m,k})$. Since the bath's spectrum should be dense, in the following we will assume that $\Gamma_m(\omega)$ becomes a continuous function with an effective bandwidth Δ_Γ [27]. Since this will restrict our further considerations to times $t - t_0 \gg 1/\Delta_\Gamma$ it should be assumed that $1/\Delta_\Gamma$ is shorter than any other relevant timescale. For simplicity of the presentation, we will consider here only the wide-band limit $\Delta_\Gamma \to \infty$ with constant $\Gamma_m(\omega) = \Gamma_m$ for all energies ω (cf. Appendix B for a discussion). ΔE refers to all possible differences of eigenenergies of the system Hamiltonian H_S while $\alpha = \pm$ refers to creation (+) and annihilation (−) processes.

The Redfield-I equation becomes

$$\partial_t \rho = -i[\widetilde{H}_S, \rho] + \widetilde{\mathcal{L}}_t\, \rho \tag{12}$$

with the new Liouville superoperator

$$\widetilde{\mathcal{L}}_t \rho = \sum_{\substack{m,\alpha \\ \Delta E,\Delta E'}} M^\alpha_m(t,\Delta E,\Delta E')\, \mathcal{L}^\alpha_m(\Delta E,\Delta E')\, \rho, \tag{13}$$

including the coefficients

$$M^\alpha_m(t,\Delta E,\Delta E') = \frac{A^\alpha_m(t,\Delta E) + \overline{A^\alpha_m(t,\Delta E')}}{2} \tag{14}$$

and the superoperators

$$\mathcal{L}^\alpha_m(\Delta E,\Delta E')\rho = K^\alpha_m(\Delta E)\, \rho\, K^\alpha_m(\Delta E')^\dagger - \tfrac{1}{2}\big\{K^\alpha_m(\Delta E')^\dagger K^\alpha_m(\Delta E), \rho\big\}. \tag{15}$$

The indices m, α refer to the effective relaxation channels. The total Liouville superoperator $\widetilde{\mathcal{L}}_t$ does not necessarily preserve the positivity of ρ, as explained in Sec. I. The coefficients $M^\alpha_m(t,\Delta E,\Delta E')$ are time dependent due to integration over a finite history between the starting point at $t = t_0$, when the system and the bath were prepared in a product state, and the current time t.

In the standard scheme, the coefficients are stabilized by the (second) Markov approximation, shifting the starting point of the evolution to $t_0 \to -\infty$. By integrating over the infinite history, the theory becomes Markovian. The coefficients reduce to constants depending only on the Fermi distribution

[2] Positivity of the superoperator $\mathcal{L}$ means the map $\mathcal{U}_t \equiv \hat{T}\,\exp\left(\int_0^t \mathrm{d}\tau\, \mathcal{L}_\tau\right)$ preserves the positivity of the density matrix $\rho(t) = \mathcal{U}_t\rho(0)$ for all $t \geqslant 0$. It is also required that $\mathcal{L}$ preserves the trace of ρ.

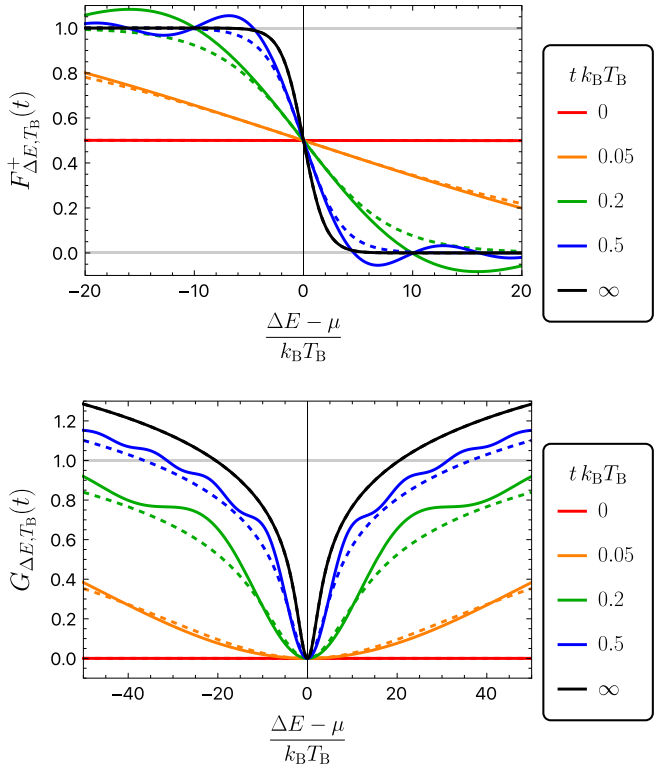

FIG. 1. Solid lines show the real part $F^{+}_{\Delta E,T_B}(t)$ (top) and the imaginary part $G_{\Delta E,T_B}(t)$ (bottom) of the coefficients $A^{+}_{m}(t,\Delta E)$ as functions of ΔE in units of $k_B T$. The dashed lines show the approximations based on the time-dependent temperature $T(t)$, the real part $\mathcal{F}^{+}_{\Delta E,T_B}(t)$ (top), and the imaginary part $\mathcal{G}_{\Delta E,T_B}(t)$ (bottom). Different colors correspond to various times t. For $t=0$ (red) and $t\to\infty$ (black), the solid and dashed lines match together. The original real parts $F^{+}_{\Delta E,T_B}(t)$ overshoot the interval [0,1] while their approximations stay within it.

of the bath leading to the Redfield-II equation. It provides the staring point for further approximations, e.g., the secular, coherent, or other approximations [26,34,36–42], leading to various versions of the GKSL equation (cf. Appendix A).

IV. TIME-DEPENDENT TEMPERATURE

A. Real part of $A^{\pm}_{m}(t,\Delta E)$

Here, we first stay with the Redfield-I equation and look closer at the time dependence of the coefficients $A^{\pm}_{m}(t,\Delta E)$. In the wide-band limit (for non-wide-band cf. Appendix B), the real part of (11) becomes

$$\Gamma_m F^{\pm}_{\Delta E,T_B}(t) = \mathrm{Re}\,A^{\pm}_{m}(t,\Delta E), \tag{16}$$

where

$$F^{\pm}_{\Delta E,T_B}(t) \equiv \frac{1}{2} \mp k_B T_B \int_0^{t-t_0} \frac{\sin[(\Delta E-\mu)\tau]}{\sinh(\pi k_B T_B \tau)} d\tau. \tag{17}$$

For $k_B T_B \lesssim |\Delta E-\mu|/4$ the factors $F^{\pm}_{\Delta E,T_B}(t)$ show excessive oscillations and become negative or larger than one for times $t\sim 1/|\Delta E-\mu|$ (cf. solid lines in Fig. 1, top). This leads to the above-mentioned problems of the Redfield equation (cf. Sec. I) resulting in violation of the positivity of the density matrix (cf. also Sec. V for particular examples).

At the initial time, $F^{\pm}_{\Delta E,T_B}(t=t_0)=\frac{1}{2}$ is independent of the energy difference ΔE and temperature T_B. This corresponds to the Fermi function $f_{\pm}(\Delta E,\infty)=\frac{1}{2}$ at infinite temperature. The Redfield equation (12) simplifies then to the GKSL equation (cf. Appendix A) coupled to infinitely hot baths with $L_{m,-}=c_m/\sqrt{2}$ and $L_{m,+}=c_m^{\dagger}/\sqrt{2}$, where $L_{m,\pm}$ are functions of c_m and $c_m^{\dagger}$ only. In case when different c_m's correspond to separate sites m then these Lindblad operators become fully local.

If $t-t_0$ is large compared to the characteristic timescale

$$\tau_c = \min\left(\frac{1}{k_B T_B}, \frac{1}{|\Delta E-\mu|}\right) \tag{18}$$

given by the smaller of the inverse thermal energy and the inverse energy distance to the chemical potential, the integral (17) converges and the coefficients

$$F^{\pm}_{\Delta E,T_B}(t\gg\tau_c) \approx f_{\pm}(\Delta E,T_B) \tag{19}$$

approach the Fermi function for the bath temperature T_B.

Our main finding, from the technical point of view, is that the integral in (17) can be uniformly in t, ΔE, and T_B approximated by the function

$$I = k_B T_B \int_0^{t-t_0} \frac{\sin[(\Delta E-\mu)\tau]}{\sinh(\pi k_B T_B \tau)} d\tau \tag{20}$$

$$\approx \frac{1}{\pi}\mathrm{Si}\left[\frac{\pi(\Delta E-\mu)}{4k_B T_B}\tanh\left(\frac{4k_B T_B(t-t_0)}{\pi}\right)\right], \tag{21}$$

with Si being the sine integral, $\mathrm{Si}(x)=\int_0^x \sin(u)/u\,du$. It relies on the astonishing similarity (C1) discussed in Appendix C 1 (cf. Fig. 8) and offers a good approximation when $T_B(t-t_0)\lesssim\pi/4$. It still shows the unwanted excess oscillations as in original $F^{\pm}_{\Delta E,T_B}(t)$ (cf. Fig. 1). These can be most clearly observed in the limit $T_B\to 0$ when (21) becomes exact

$$I = \int_0^{t-t_0} d\tau \frac{\sin[(\Delta E-\mu)\tau]}{\pi\tau} = \frac{\mathrm{Si}[(\Delta E-\mu)(t-t_0)]}{\pi} \tag{22}$$

and can assume values out of the range $[-\frac{1}{2},\frac{1}{2}]$ which may lead to negative values of $F^{\pm}_{\Delta E,T_B}(t)$ in (17). Therefore, in the last step, we replace the sine integral function by tanh which has a similar form but stays bounded in the proper region without any oscillations (cf. Fig. 10), by which we arrive at

$$I \approx \frac{1}{2}\tanh\left[\frac{\Delta E-\mu}{2k_B T_B}\tanh\left(\frac{4k_B T_B(t-t_0)}{\pi}\right)\right] \tag{23}$$

(cf. Appendix C 2 for the full derivation).

In the limit $t\to\infty$, the approximation (23) becomes an equality [with the inner $\tanh(\infty)=1$] and inserted into (17) delivers[3] the static Fermi function (19). By inserting the full approximation obtained in (23) into the formula (17) and denoting the approximated coefficients as $\mathcal{F}^{\pm}_{\Delta E,T_B}(t)$ we find that the result can be recast as a Fermi function, too (cf. Fig. 1, top)

$$F^{\pm}_{\Delta E,T_B}(t) \approx \mathcal{F}^{\pm}_{\Delta E,T_B}(t) \equiv F^{\pm}_{\Delta E,T(t)}(\infty) = f_{\pm}(\Delta E,T(t)), \tag{24}$$

[3]Due to the identity $\frac{1}{2}\mp\frac{1}{2}\tanh[(\Delta E-\mu)/(2k_B T_B)] = f_{\pm}(E,T_B)$.

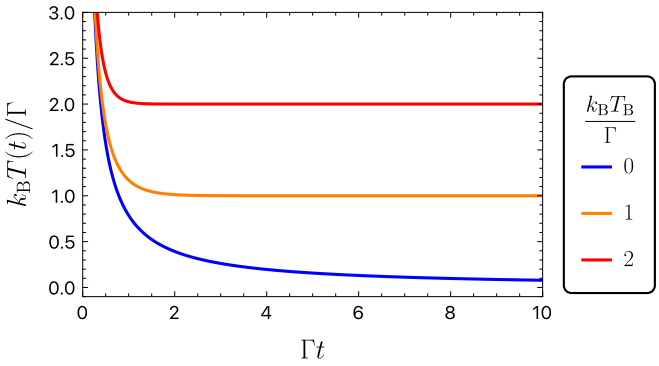

FIG. 2. Evolution of the time-dependent effective temperature $T(t)$ for various temperatures of the bath T_B.

now with a modified, time-dependent temperature

$$T(t) = T_B \Big/ \tanh\left(\frac{4k_B T_B}{\pi}(t - t_0)\right) \tag{25}$$

(cf. Fig. 2).

The effective temperature $T(t)$ is universal, i.e., independent of ΔE. It diverges at short times,

$$T(t) \approx \frac{\pi}{4k_B(t - t_0)} \equiv T_0(t) \quad \text{for} \quad t - t_0 \ll \frac{1}{k_B T_B} \tag{26}$$

and converges to the true bath temperature $T(t) \to T_B$ for late times $t \to \infty$ (cf. Fig. 2). We will refer to it as the time-dependent effective bath temperature, for it is described by the effective bath temperature from the perspective of the system. The origin of its time dependence is in the contact of the system with the environment at $t = t_0$ and the buildup of correlations (which were assumed to be absent for $t < t_0$). It originates in short time off–resonant (virtual) transition processes between the bath and the system involving an energy range close to the Fermi–level, proportional to the inverse of the characteristic time of the associated oscillations, which scales as $(t - t_0)^{-1}$, staying independent of other parameters, such as Γ or T_B. Also for later times, $T(t)$ cannot depend on the coupling strength Γ because we keep only the lowest-order terms in (7) and hence Γ automatically factorizes in (11) and (16) and plays only the role of a scaling factor.

The approximate coefficients directly satisfy three important limiting cases, for $t \to \infty$, $t \to 0$, and $T_B \to \infty$, which can be directly obtained from the integral (17) and the fourth limiting case, for $T_B \to 0$, which resolves the problem of excess oscillations observed in (22) and replaces the result with a nonoscillatory function,

$$\begin{aligned}
\mathcal{F}^{\pm}_{\Delta E, T_B}(t \to \infty) &= \frac{1}{2} \mp \frac{1}{2} \tanh \frac{\Delta E - \mu}{2k_B T_B} = f_{\pm}(\Delta E, T_B), \\
\mathcal{F}^{\pm}_{\Delta E, T_B}(t \to 0) &= \frac{1}{2} = f_{\pm}(\Delta E, \infty), \\
\mathcal{F}^{\pm}_{\Delta E, T_B \to \infty}(t) &= \frac{1}{2} = f_{\pm}(\Delta E, \infty), \\
\mathcal{F}^{\pm}_{\Delta E, T_B \to 0}(t) &= \frac{1}{2} \mp \frac{1}{2} \tanh \frac{2(\Delta E - \mu)(t - t_0)}{\pi} \\
&= f_{\pm}(\Delta E, T_0(t)),
\end{aligned} \tag{27}$$

where $T_0(t)$ is given in (26). In all cases $\mathcal{F}^{\pm}_{\Delta E, T_B}(t)$ stays in the required range [0,1] (cf. dashed lines in Fig. 1, top).

B. Imaginary part of $A^{\pm}_m(t, \Delta E)$

After we have considered the real part of $A^{\pm}_m(t, \Delta E)$ we next focus on its imaginary part. In the wide-band limit, $\mathrm{Im}\, A^{\pm}_m(t, \Delta E)$ diverges. However, (9) and (14) contain only differences, $\mathrm{Im}\, A^{\pm}_m(t, \Delta E) - \mathrm{Im}\, A^{\pm}_m(t, \Delta E')$, which are finite. Therefore, we define

$$\Gamma_m G_{\Delta E, T_B}(t) = \mathrm{Im}\, A^{\pm}_m(t, \Delta E) - \mathrm{Im}\, A^{\pm}_m(t, \mu) \tag{28}$$

(which is independent of $\pm$) by choosing a universal value $\Delta E' = \mu$ for the counterterm and obtain

$$G_{\Delta E, T_B}(t) \equiv k_B T_B \int_0^{t - t_0} \frac{1 - \cos[(\Delta E - \mu)\tau]}{\sinh(\pi k_B T_B \tau)} d\tau. \tag{29}$$

Applying similar approximations as for the real part of $A^{\pm}_m(t, \Delta E)$ we find

$$G_{\Delta E, T_B}(t) \approx \frac{1}{\pi} \mathrm{Re}\left[\psi\left(\frac{1}{2} + i\frac{\Delta E - \mu}{2\pi k_B T(t)}\right) - \psi\left(\frac{1}{2}\right)\right] \tag{30}$$

with the same effective temperature $T(t)$ as in (25) (cf. Fig. 1 and Appendix C 3) and $\psi(x)$ the digamma function [55, Sec. 6.3]. Denoting the right-hand side by $\mathcal{G}_{\Delta E, T_B}(t)$, we arrive, in full analogy to (24), at

$$G_{\Delta E, T_B}(t) \approx \mathcal{G}_{\Delta E, T_B}(t) \equiv G_{\Delta E, T(t)}(\infty). \tag{31}$$

This confirms that the same effective temperature $T(t)$ can be used in both the real and the imaginary parts of $A^{\pm}_m(t, \Delta E)$.

In the next two sections, V and VI, we will consider a simple system consisting of a single quantum dot in order to compare the different approaches analytically and numerically:

(i) exact solutions (for the noninteracting system);

(ii) Redfield-I equation with time-dependent coefficients $F^{\pm}_{\Delta E, T_B}(t)$ leading to positivity problem 1 due to overshooting the range [0,1];

(iii) modified Redfield-I equation with approximate coefficients $\mathcal{F}^{\pm}_{\Delta E, T_B}(t) \in [0, 1]$ based on time-dependent temperature $T(t)$;

(iv) Redfield-II equation with static coefficients $F^{\pm}_{\Delta E, T_B}(\infty) \in [0, 1]$,

summarized in Table I. We will concentrate only on the real part $F^{\pm}_{\Delta E, T_B}(t)$ since the imaginary part $G_{\Delta E, T_B}(t)$ will not be significant for that system. For larger systems than one quantum dot, we would also deal with the problem 2 of nonpositivity of some 2×2 matrix valued coefficients, $\mathcal{M} \not\geqslant 0$, in which case we might want to further approximate the Redfield-I and -II equations to the Lindblad form with modified $\widetilde{\mathcal{M}} \geqslant 0$ (cf. Appendix A).

V. EXAMPLE: SINGLE QUANTUM DOT

Here, we consider a simple system to demonstrate the application of the above proposed approximation method based on the time-dependent temperature. We choose a single quantum dot described by the Anderson impurity model [56]

$$H_S = U n_\uparrow n_\downarrow + \varepsilon(n_\uparrow + n_\downarrow) \tag{32}$$

TABLE I. Overview of the discussed approximation schemes. The constants μ and t_0 were set to zero for brevity.

Approach	Coefficients	Value	For $T_\mathrm{B}=0$
Redfield-I	$F^{\pm}_{\Delta E,T_\mathrm{B}}(t)$		$\frac{1}{2}\mp\mathrm{Si}(\Delta E t)/\pi$
Modified Redfield-I	$\mathcal{F}^{\pm}_{\Delta E,T_\mathrm{B}}(t)=f_{\pm}(\Delta E,T(t))$	$\frac{1}{2}\mp\frac{1}{2}\tanh\left[\frac{\Delta E}{2k_\mathrm{B}T_\mathrm{B}}\tanh\left(\frac{4k_\mathrm{B}T_\mathrm{B}t}{\pi}\right)\right]$	$\frac{1}{2}\mp\frac{1}{2}\tanh\left(\frac{2\Delta E t}{\pi}\right)$
Static Redfield-II	$F^{\pm}_{\Delta E,T_\mathrm{B}}(\infty)=f_{\pm}(\Delta E,T_\mathrm{B})$	$\frac{1}{2}\mp\frac{1}{2}\tanh\left(\frac{\Delta E}{2k_\mathrm{B}T_\mathrm{B}}\right)$	$\Theta(-\Delta E)$

with $n_s=c_s^\dagger c_s$, spin $s=\uparrow,\downarrow$, Coulomb interaction $U>0$, and onsite energy ε, satisfying $-U<\varepsilon-\mu<0$. The system has $\dim(S)=4$ eigenstates [cf. (2)] and is connected to $M=2$ baths with different spin polarizations [cf. (3) and (4)]. Both in the static (second) Markov approximation, for $t_0\to-\infty$, as well as in the time-dependent effective temperature approximation, with $t_0=0$, (12) reduces to a GKSL equation (cf. Appendix A) with the Lindblad dissipators (A5) or (A7) (which differ only by nonphysical coherences between states with different occupation numbers)

$$L^{\pm}_{s,1}=\sqrt{f_{\pm}(\varepsilon,\widetilde{T}(t))}\,c_s^{\pm}(1-n_{\bar{s}}), \tag{33}$$

$$L^{\pm}_{s,2}=\sqrt{f_{\pm}(\varepsilon+U,\widetilde{T}(t))}\,c_s^{\pm}n_{\bar{s}}, \tag{34}$$

for tunneling in or out ($\pm$) of the first (33) and second electron (34) with spin s. The temperature $\widetilde{T}(t)$ in the Fermi functions $f_\pm$ is either constant and equal T_B or time dependent as given by (25). In the static case, for $T_\mathrm{B}=0$, the states $|\uparrow\rangle\langle\uparrow|$ and $|\downarrow\rangle\langle\downarrow|$ are "frozen." However, the time-dependent effective temperature $T(t)$, even for $T_\mathrm{B}=0$, becomes initially large, $T(t\approx0)\to\infty$ [cf. (26)] and the system is temporarily driven towards the fully mixed "hot" state

$$\rho_\infty=\frac{1}{4}\Big[|0\rangle\langle0|+|\uparrow\rangle\langle\uparrow|+|\downarrow\rangle\langle\downarrow|+|\uparrow\downarrow\rangle\langle\uparrow\downarrow|\Big]. \tag{35}$$

Eventually, as $T(t)\to T_\mathrm{B}=0$, it relaxes to some mixture $a|\uparrow\rangle\langle\uparrow|+b|\downarrow\rangle\langle\downarrow|$ with $a+b=1$. Starting with the pure state $|\uparrow\rangle\langle\uparrow|$, the final spin-$z$ $\langle S_z\rangle=(a-b)/2$ will measure how strong the influence of the "hot" period on the effective dynamics was. This observable satisfies an autonomous differential equation[4] (valid for any T_B)

$$\dot{S}_z^{\mathrm{eff}}(t)=-\Gamma\Big[1-f_+(\varepsilon,T(t))+f_+(\varepsilon+U,T(t))\Big]S_z^{\mathrm{eff}}(t) \tag{36}$$

which can be integrated to

$$S_z^{\mathrm{eff}}(t)=S_z(0)\exp\left[-2\Gamma\int_0^t \mathrm{d}t' f_+(\varepsilon+U,T(t'))\right], \tag{37}$$

where we have chosen the special value $\varepsilon=\mu-U/2$ for convenience. For $T_\mathrm{B}>0$ this integral is difficult to calculate but it diverges for $t\to\infty$ and thus leads to $S_z(\infty)=0$. For $T_\mathrm{B}=0$, we have $k_\mathrm{B}T(t)=\pi/(4t)$ [cf. (25)] and this integral can be calculated exactly to give

$$S_z^{\mathrm{eff}}(t)=S_z(0)\,e^{-2\Gamma t}\left(1+e^{\frac{2U}{\pi}t}\right)^{\frac{\Gamma\pi}{U}}2^{-\pi\frac{\Gamma}{U}} \tag{38}$$

which for $t\gg1/U$ has the limit

$$S_z^{\mathrm{eff}}(t)\cong 2^{-\pi\Gamma/U}S_z(0). \tag{39}$$

It means that the initial spin-z, $S_z(0)$, decays in a nonperturbative way, which is enhanced by the system-bath coupling Γ and suppressed by the Coulomb repulsion U. This is in contradiction to the observation that both pure states are "frozen" in the static (second) Markov case.

Also for the not approximated Redfield-I master equation (12) the spin-z can be calculated analogously to (37)

$$S_z(t)=S_z(0)\exp\left[-2\,\Gamma\int_0^t F^{+}_{\Delta E=\varepsilon+U,T_\mathrm{B}}(t')\,dt'\right]. \tag{40}$$

In this particular system and for $T_\mathrm{B}=0$ the integral can be evaluated exactly and gives

$$S_z(t)=S_z(0)\,e^{-\Gamma t}\exp\left\{\frac{4\,\Gamma}{\pi U}\left[\cos\left(\frac{Ut}{2}\right)-1\right]+\frac{2\,\Gamma\,t}{\pi}\mathrm{Si}\left(\frac{Ut}{2}\right)\right\} \tag{41}$$

which for $t\gg1/U$ gives

$$S_z(t)\cong e^{-4\,\Gamma/(\pi U)}S_z(0). \tag{42}$$

Due to $2^{-\pi\Gamma/U}<e^{-4\,\Gamma/(\pi U)}$, the approximation with the effective temperature (39) slightly overestimates the effect compared to the prediction of the Redfield-I master equation (42), however, both stay within the same order of magnitude which justifies the effective temperature approximation (cf. Fig. 3). On the other hand, the Redfield-I master equation (12) does not preserve the positivity of the density matrix (cf. Sec. IV) and leads to negative probability, as shown in Fig. 3 (second from bottom) whereas the effective temperature approximation is free of this problem. For bath temperatures $T_\mathrm{B}>0$, both results decay to $S_z(\infty)=0$ at late times. However, at short times, $t\ll\tau_\mathrm{c}$, and small bath temperature T_B, the Redfield-I master equation and the effective temperature approximation give $S_z(t)\sim\exp(-\Gamma t)$ while in the static approximation the decay is exponentially suppressed, $S_z(t)\sim\exp\left(-2\,\Gamma e^{-U/(2k_\mathrm{B}T_\mathrm{B})}t\right)$.

By a similar mechanism, the effective temperature can even lead to an excitation of the ground state and deposit energy into the system. By adding a magnetic field in the z direction with the Hamiltonian $H_z=2BS_z$ we obtain together with (32)

$$H_S=Un_\uparrow n_\downarrow+(\varepsilon+B)n_\uparrow+(\varepsilon-B)n_\downarrow \tag{43}$$

and lift the degeneracy between the $|\uparrow\rangle$ and $|\downarrow\rangle$ states. We choose $T_\mathrm{B}=0$ and start in the ground state $\rho_S(0)=|\uparrow\rangle\langle\uparrow|$ (for $B<0$). By connecting the system with the bath at

[4] If $\widetilde{\mathcal{L}}_t^\dagger$ is time dependent, $\dot{A}_\mathrm{H}(t)=\widetilde{\mathcal{L}}_t^\dagger A_\mathrm{H}(t)$ is generally not correct for any operator A_H in the Heisenberg picture. However, if the equation is autonomous, then it holds true.

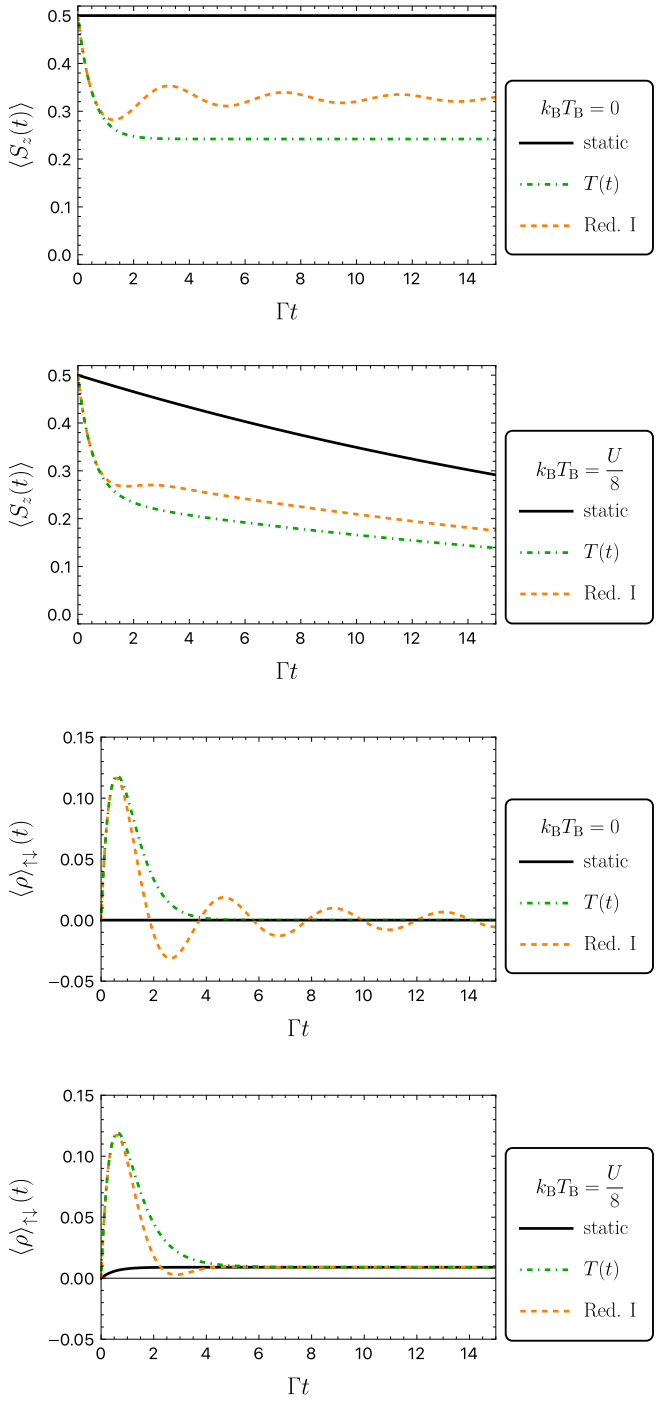

FIG. 3. One quantum dot. Top pair: spin $\langle S_z(t)\rangle$ as a function of time for the static Markov and the effective temperature approximations as well as for the Redfield-I master equation (12). The Coulomb interaction is $U = 3\,\Gamma$, the on-site potential is $\varepsilon = \mu - \frac{U}{2}$, and the bath temperature is $T_B = 0$ or $k_B T_B = U/8$. The initial state is $\rho_S(0) = |\uparrow\rangle\langle\uparrow|$. Bottom pair: probability of the double occupation $\langle\rho\rangle_{\uparrow\downarrow}(t) \equiv \langle\uparrow\downarrow|\rho(t)|\uparrow\downarrow\rangle$ as a function of time, here identical with the zero occupation $\langle\rho\rangle_0(t) \equiv \langle 0|\rho(t)|0\rangle$. Both can get negative for the Redfield equation. The energy, given by $\langle H_S - \mu N\rangle = U[\langle\rho\rangle_{\uparrow\downarrow} + \langle\rho\rangle_0 - 1]/2$ with $N = n_\uparrow + n_\downarrow$, also swings below its theoretical lower limit $-U/2$ for $T_B = 0$. The parameters are the same as for $\langle S_z(t)\rangle$, respectively.

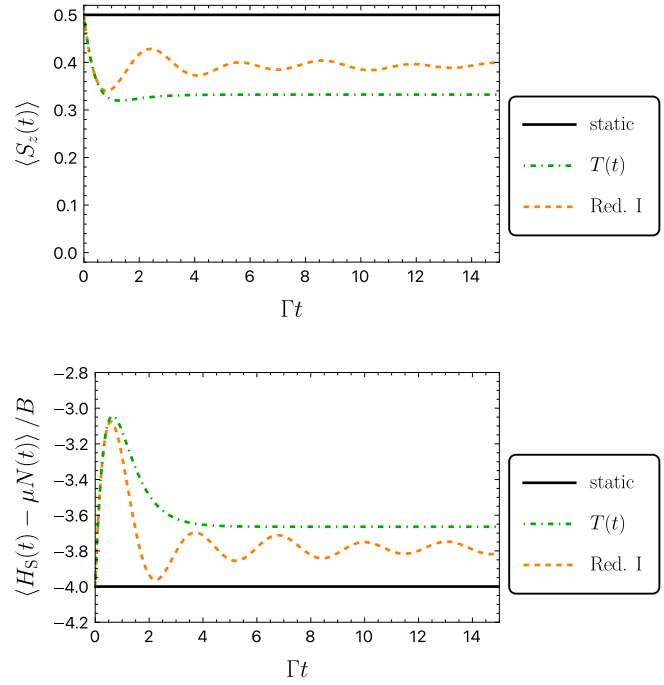

FIG. 4. One quantum dot. Spin $\langle S_z(t)\rangle$ (top) and energy $\langle H_S(t) - \mu N(t)\rangle$ with $N = n_\uparrow + n_\downarrow$ (bottom) as functions of time for the static Markov and the effective temperature approximations as well as for the Redfield-I master equation (12). The Coulomb interaction is $U = 3\,\Gamma$, the onsite potential is $\varepsilon = \mu - U/2$, the bath temperature is $T_B = 0$, the magnetic field is $B = -\Gamma/2$, and the initial state is $\rho_S(0) = |\uparrow\rangle\langle\uparrow|$ (ground state).

$t = t_0 = 0$, due to the high effective temperature $T(t)$ at short times, there will be an increase of energy in the system

$$\Delta H_S = H_S(\infty) - H_S(0) = 2B[S_z(\infty) - S_z(0)] \tag{44}$$

(cf. Fig. 4). Although the bath and the system were initially in their respective ground states, the increase of energy, ΔH_S, results from the coupling Hamiltonian H_C. In the limit of weak B, it can be evaluated to

$$\Delta H_S = |B|\left(1 - e^{-4\,\Gamma/(\pi U)}\right) + O\left(\frac{B^2}{U}\right) \tag{45}$$

for the Redfield-I master equation (12) and to

$$\Delta H_S = |B|\left(1 - 2^{-\pi\Gamma/U}\right) + O\left(\frac{B^2}{U}\right) \tag{46}$$

for the effective temperature approximation, where again the latter method slightly overestimates the result.

VI. NONINTERACTING QUANTUM DOT AS BENCHMARK

Since the proposed effective temperature method is an approximation to the Redfield equation which in turn is also an approximation itself, it does not provide a proper benchmark for testing the accuracy. Especially in the situations when the Redfield equation leads to mathematical problems the comparison is unclear. Therefore, we consider here the noninteracting case with $U = 0$ which is exactly

solvable and compare the different master-equation approaches with it.

Without the Coulomb interaction, the system splits into two identical copies of a spinless system

$$H = \varepsilon\, n + \sum_k (\gamma_k c^\dagger\, b_k + \text{H.c.}) + \sum_k \varepsilon_k b_k^\dagger b_k \qquad (47)$$

with $n = c^\dagger c$. Starting from the Heisenberg equation of motion and Laplace transformation technique [8,10], it is possible to express the annihilation operator of the dot in the Heisenberg picture

$$c_{\mathrm{H}}(t) = e^{-i\varepsilon t - \frac{\Gamma}{2}t} c_{\mathrm{H}}(0) + \sum_k \gamma_k b_k \left(\frac{e^{-i\varepsilon t - \frac{\Gamma}{2}t} - e^{-i\varepsilon_k t}}{(\varepsilon - \varepsilon_k) - i\frac{\Gamma}{2}} \right) \qquad (48)$$

in terms of the operators $c = c_{\mathrm{H}}(0)$ and b_k in the Schrödinger picture. Assuming an initial product state between the dot and a Fermi distributed bath leads to

$$\langle n(t)\rangle = e^{-\Gamma t}\langle n(0)\rangle + \Gamma \int_{-\infty}^{\infty} \frac{\mathrm{d}\omega}{2\pi} f_+(\omega + \varepsilon, T_{\mathrm{B}}) \frac{e^{-\Gamma t} + 1 - 2\,\cos(\omega t) e^{-\frac{\Gamma}{2}t}}{\omega^2 + \frac{\Gamma^2}{4}}. \qquad (49)$$

Figure 5 compares the exact solution (49) and the different master equations as functions of time. Due to forbidden energy transitions for $\varepsilon > \mu$ and $T_{\mathrm{B}} = 0$, the static approximation leads to no dynamics when starting with an initially empty dot while in all other approaches we observe relaxation at short times $t \lesssim \tau_{\mathrm{c}}$. Similarly to Fig. 4, in Fig. 5 we observe an energy gain $(\varepsilon - \mu)[\langle n(t)\rangle - \langle n(0)\rangle]$ in the system which originates from the coupling term in the Hamiltonian H_C (in Appendix D, we discuss this in more detail). By comparing the exact solution with the results of the different master equations, we find that both time-dependent Redfield-I master equations, original and modified with the effective temperature, are accurate for times shorter than the characteristic timescale τ_{c} (18) (cf. Fig. 6). The accuracy for short times holds still true even in the case of strong coupling $\Gamma \gtrsim |\mu - \varepsilon|$, where the exact solutions show significant deviations from all Redfield master equations at late times $t \gg \tau_{\mathrm{c}}$ (cf. Fig. 6).

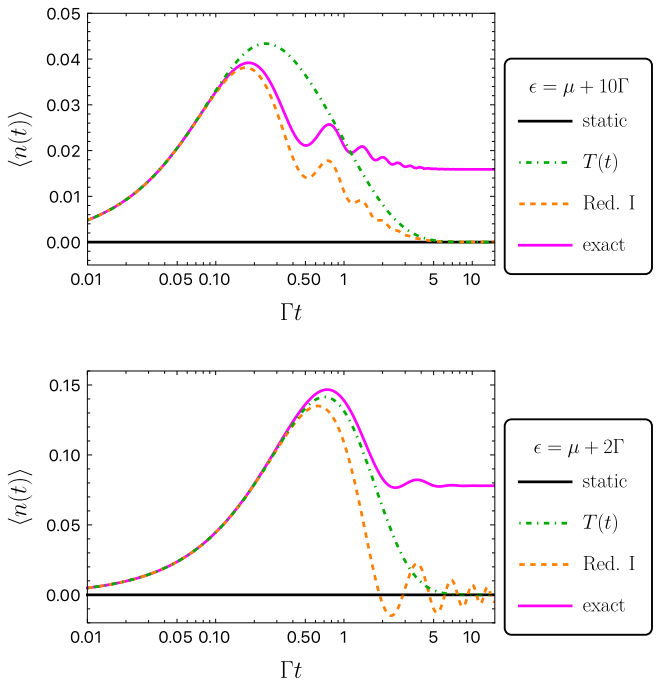

FIG. 5. Particle number $\langle n(t)\rangle$ as a function of time (logarithmic scale). The lines show the various master equations and exact solution (49) with $T_{\mathrm{B}} = 0$, $U = 0$, $\langle n(0)\rangle = 0$ and $\varepsilon = \mu + 10\,\Gamma$ (top) or $\varepsilon = \mu + 2\,\Gamma$ (bottom).

In the regime of intermediate times and strong coupling Γ, the original Redfield-I master equation may lead to nonphysical values of the particle number below zero or above one [cf. Fig. 5 (bottom)] where the Redfield-I master equation modified with $T(t)$ is superior (cf. Fig. 6). The opposite happens for weak coupling $\Gamma \ll |\mu - \varepsilon|$ [cf. Fig. 5 (top) and Fig. 6] where the effective temperature method overshoots, as discussed in Sec. V. However, the differences between all master equations and the exact solution vanish in that regime as $\Gamma\tau_{\mathrm{c}} = \frac{\Gamma}{|\mu-\varepsilon|} \to 0$ [cf. Fig. 6 (inset)].

The above considerations extend qualitatively to the regime $k_{\mathrm{B}}T_{\mathrm{B}} \ll \frac{|\mu-\varepsilon|}{4}$ where the largest deviations between different approaches are expected. In contrary, for temperatures $k_{\mathrm{B}}T_{\mathrm{B}} \gtrsim \frac{|\mu-\varepsilon|}{4}$, the original Redfield-I master equation no longer reaches nonphysical values of the particle number and becomes similar to the modified Redfield-I master equation. Analogously to $T_{\mathrm{B}} = 0$, the differences between the master equations and the exact solution vanish in the regime of high T_{B} as $\Gamma\tau_{\mathrm{c}} = \frac{\Gamma}{k_{\mathrm{B}}T_{\mathrm{B}}} \to 0$.

VII. CONCLUSIONS

We considered a fermionic quantum system exchanging particles with a thermal bath at fixed temperature T_{B}. By eliminating the bath from the description we derived an approximation of the first Redfield equation with time-dependent coefficients which offers the interpretation of a time-dependent effective temperature $T(t)$ (25). For times smaller than the characteristic time τ_{c} (18), the effective temperature is very large, $T(t) \to \infty$, which can be explained by the fact that at short timescales all energetically forbidden transitions are allowed.[5] At timescales much larger than τ_{c}, the effective temperature $T(t)$ converges against the true environment temperature T_{B}. The use of the effective temperature

[5] An entirely different approach [57], based on the renormalization flow in the environment's temperature, demonstrated that the short-time dynamics of observables shows a universal temperature-independent behavior when the metallic reservoirs have a flat wide band. This is in a perfect agreement with our observation of infinite effective temperature which makes the renormalization flow trivial.

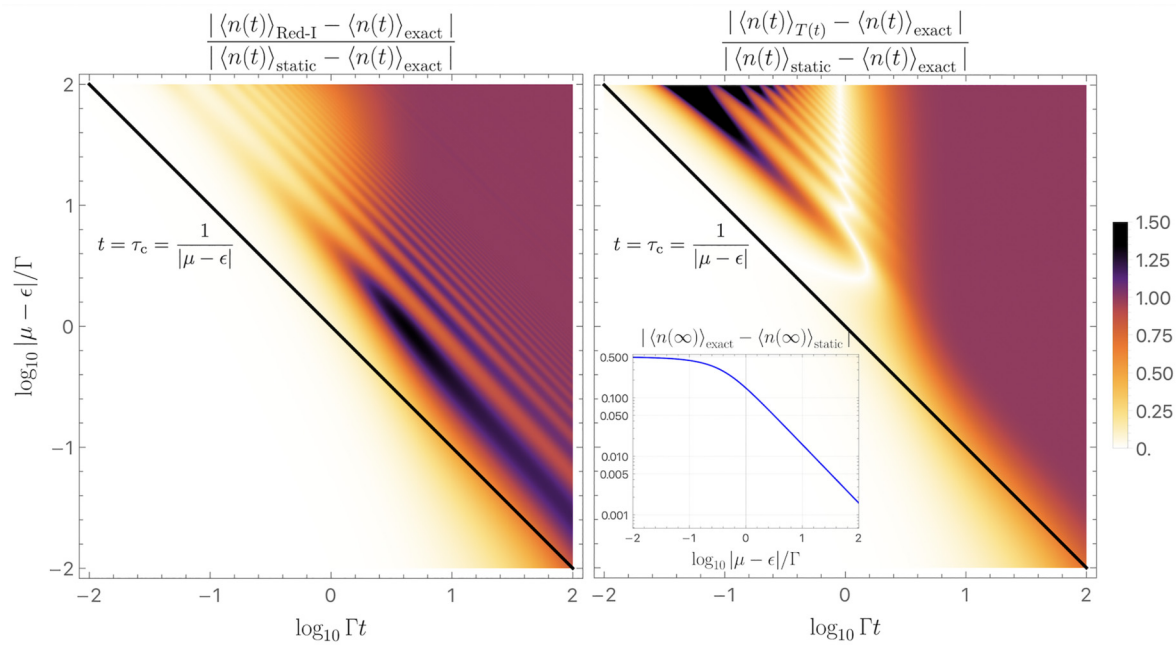

FIG. 6. The normalized difference of the particle number between the exact solution (49) and the Redfield-I equation (left panel) or the Redfield-I equation modified with $T(t)$ (right panel) as a function of time and of the difference between the chemical potential μ and the onsite potential ε (both in logarithmic scales). The normalization is given by the difference between the exact and the static result. For both situations (left and right), the normalized and non-normalized deviations are small if the time is smaller than the characteristic timescale τ_c. The black line shows the correspondence between τ_c and $|\mu - \varepsilon|$. The inset shows the non-normalized deviation between the particle number of the steady state of the static Redfield master equation and the exact solution as a function of time. This value decays as $|\langle n(\infty)\rangle_{\text{exact}} - \langle n(\infty)\rangle_{\text{static}}| \approx \Gamma/(2\pi|\mu - \varepsilon|)$ and vanishes in the weak coupling limit. The system is described by (47) with bath temperature $T_B = 0$.

$T(t)$ fixes also the problems of nonpositivity in the development of the density matrix by the Redfield equation.

We demonstrated these effects on the example of a single quantum dot with Coulomb interaction (Sec. V) which we also compared with exact solutions for a system without the Coulomb interaction, using it as a benchmark (Sec. VI). In both cases we have shown a qualitative and quantitative agreement between the solutions of the original time-dependent Redfield master equation and its approximation based on the time-dependent temperature. In the case without the Coulomb interaction, we have shown a good agreement between the solutions of the Redfield equations and the exact solution. For short times, we see a perfect agreement even for parameters for which the Redfield approximation generally does not hold at later times. This confirms that the effective temperature scheme offers an approximation which is as close to the exact solution as the original Redfield equation and combines a perfect match at short times with being free of any mathematical flaws at later times.

Previous versions of time-dependent effective temperatures discussed in the literature [47–53] differ substantially from the approach presented here. Most of them are related to time-dependent quasiequilibrium temperatures of the system or of the bath, based on their internal dynamics. In contrast, in our approach the bath stays in thermal equilibrium at T_B and the *effective bath temperature* $T(t)$ refers to its observed value from the perspective of the system, emerging as a consequence of switching on the interaction and buildup of correlations between the system and the bath. Our approach is based on a sophisticated analytic approximation holding for a wide range of temperatures T_B, energies ΔE, and timescales t (23)–(25), and agrees with the Redfield-I equation when $t - t_0 \lesssim \tau_c$ (18). Despite this, it preserves the original structure of the standard static results (24), replacing only T_B with $T(t)$ which, among others, can be practical in numerical simulations.

The method of time-dependent effective bath temperature leaves open space for further approximations and, therefore, can be applied to various types of originally time-independent master equations, beyond the secular approximation or time-averaging methods. Its potential application to bosonic environments remains open due to the qualitative differences between the Bose and the Fermi statistics.

ACKNOWLEDGMENTS

The authors thank G. Schaller for fruitful discussions and valuable feedback on the manuscript. We gratefully acknowledge funding by the Deutsche Forschungsgemeinschaft (DFG, German Research Foundation)–Project No. 278162697–SFB 1242.

APPENDIX A: FROM REDFIELD TO LINDBLAD

In the derivation of the Redfield-I equation (8) (cf. Sec. III), at the lowest order in the system-environment coupling strength, the preservation of positivity of the density matrix in

the evolution gets lost. Here, we discuss its corrections leading towards GKSL master equations [1,26,28,34,36–38].

$$\mathcal{M}^{\pm}_{\Delta E,\Delta E'}(t)=\begin{pmatrix} M_{\pm}(t,\Delta E,\Delta E), & M_{\pm}(t,\Delta E,\Delta E') \\ M_{\pm}(t,\Delta E',\Delta E), & M_{\pm}(t,\Delta E',\Delta E')\end{pmatrix}$$
$$=\begin{pmatrix} F^{\pm}_{\Delta E,T_{\mathrm{B}}}(t), & \frac{1}{2}\left[F^{\pm}_{\Delta E,T_{\mathrm{B}}}(t)+F^{\pm}_{\Delta E',T_{\mathrm{B}}}(t)\right]+\frac{i}{2}\left[G_{\Delta E,T_{\mathrm{B}}}(t)-G_{\Delta E',T_{\mathrm{B}}}(t)\right] \\ \frac{1}{2}\left[F^{\pm}_{\Delta E,T_{\mathrm{B}}}(t)+F^{\pm}_{\Delta E',T_{\mathrm{B}}}(t)\right]-\frac{i}{2}\left[G_{\Delta E,T_{\mathrm{B}}}(t)-G_{\Delta E',T_{\mathrm{B}}}(t)\right], & F^{\pm}_{\Delta E',T_{\mathrm{B}}}(t)\end{pmatrix} \tag{A1}$$

built with $M_{\pm}(t,\Delta E,\Delta E')\equiv M^{\pm}_{m}(t,\Delta E,\Delta E')/\Gamma_m$ independent of m [the coefficients F and G are defined in (17) and (29), respectively]. If the coefficients $F^{\pm}_{\Delta E,T_{\mathrm{B}}}(t)$ become negative (cf. Fig. 1) the blocks $\mathcal{M}$ cease to be positive definite that translates also into the total Liouville operator (13). Therefore, we propose in this work the approximation (24) which replaces them with new coefficients $\mathcal{F}^{\pm}_{\Delta E,T_{\mathrm{B}}}(t)\in[0,1]$. For consistency, we also replace the $G^{\pm}_{\Delta E,T_{\mathrm{B}}}(t)$ coefficients with $\mathcal{G}^{\pm}_{\Delta E,T_{\mathrm{B}}}(t)$ according to (31) (cf. Sec. IV).

However, in general, also the approximated matrices $\mathcal{M}^{\pm}_{\Delta E,\Delta E'}(t)$ are not positive definite for $\Delta E\neq\Delta E'$, having one positive and one negative eigenvalue, which presents another possible reason for the nonpositivity of the total Liouville operator (13).

1. Secular approximation

The off-diagonal elements of $\mathcal{M}^{\pm}_{\Delta E,\Delta E'}(t)$ correspond to coherences between states with different energies (in the Liouville space), which oscillate in time. The secular approximation [1,28] averages out the oscillations and effectively removes the off-diagonal terms by which

$$\mathcal{M}^{\pm,\mathrm{sec}}_{\Delta E,\Delta E'}(t)=\begin{pmatrix}\mathcal{F}^{\pm}_{\Delta E,T_{\mathrm{B}}}(t) & 0\\ 0 & \mathcal{F}^{\pm}_{\Delta E',T_{\mathrm{B}}}(t)\end{pmatrix} \tag{A2}$$

are obviously positive definite. It is equivalent to the replacement of the coefficients $M^{\pm}_{m,s}$ in (14) with

$$M^{\mathrm{sec}}_{\pm}(t,\Delta E,\Delta E')=\delta_{\Delta E,\Delta E'}\mathcal{F}^{\pm}_{\Delta E,T_{\mathrm{B}}}(t). \tag{A3}$$

The Liouville superoperator (13) reduces then to the Lindblad form which preserves positivity.

$$\widetilde{\mathcal{L}}\,\rho=\left[\sum_{m,\alpha\Delta E}L^{\alpha}_{m}(\Delta E)\,\rho\,L^{\alpha}_{m}(\Delta E)^{\dagger}-\frac{1}{2}\left\{L^{\alpha}_{m}(\Delta E)^{\dagger}L^{\alpha}_{m}(\Delta E),\rho\right\}\right] \tag{A4}$$

with the secular Lindblad jump operators

$$L^{\pm,\mathrm{sec}}_{m}(t,\Delta E)=\sqrt{\Gamma_m}\sum_{i,j}\delta_{\pm\Delta E,E_i-E_j}$$
$$\times\sqrt{\mathcal{F}^{+}_{E_i-E_j,T_{\mathrm{B}}}(t)}\,|E_i\rangle\langle E_i|c^{\pm}_{m}|E_j\rangle\langle E_j| \tag{A5}$$

defined for each energy difference $\Delta E=E_i-E_j$ appearing in the spectrum of the Hamiltonian H_S. The double sum runs over all eigenstates $|E_l\rangle$ of the system Hamiltonian H_S with eigenenergies E_l. As we see, the secular approximation automatically removes the imaginary parts $G_{\Delta E,T_{\mathrm{B}}}(t)$.

For transition processes in the system involving the energy differences ΔE and $\Delta E'$, we consider the blocks

2. Coherent approximation

Because the secular approximation removes too much information and can miss important physics, we developed in [26,34], along the lines of [35–38], the *coherent approximation* as the least invasive method of restoring positivity. The arithmetic mean of the real parts in the off-diagonal terms of $\mathcal{M}^{\pm}_{\Delta E,\Delta E'}(t)$ is replaced by the geometric mean while the imaginary parts are removed[6]

$$\mathcal{M}^{\pm,\mathrm{coh}}_{\Delta E,\Delta E'}(t)$$
$$=\begin{pmatrix}\mathcal{F}^{\pm}_{\Delta E,T_{\mathrm{B}}}(t), & \sqrt{\mathcal{F}^{\pm}_{\Delta E,T_{\mathrm{B}}}(t)\mathcal{F}^{\pm}_{\Delta E',T_{\mathrm{B}}}(t)}\\ \sqrt{\mathcal{F}^{\pm}_{\Delta E,T_{\mathrm{B}}}(t)\mathcal{F}^{\pm}_{\Delta E',T_{\mathrm{B}}}(t)}, & \mathcal{F}^{\pm}_{\Delta E',T_{\mathrm{B}}}(t)\end{pmatrix}. \tag{A6}$$

In this way, the negative eigenvalue gets shifted up to zero while the diagonal elements, directly influencing energy populations, stay untouched. The Liouville operator (A4) is then given in terms of the *coherent* Lindblad jump operators

$$L^{\pm,\mathrm{coh}}_{m}(t)=\sqrt{\Gamma_m}\sum_{i,j}\sqrt{\mathcal{F}^{+}_{E_i-E_j,T_{\mathrm{B}}}(t)}\,|E_i\rangle\langle E_i|c^{\pm}_{m}|E_j\rangle\langle E_j|. \tag{A7}$$

They are equal to coherent sums of the secular jump operators $L^{\pm,\mathrm{coh}}_{m}(t)=\sum_{\Delta E}L^{\pm,\mathrm{sec}}_{m}(t,\Delta E)$ over the spectrum of the energy differences which motivates their name. For more details regarding their derivation and discussion of their properties we refer to [34, Appendix A].

APPENDIX B: BEYOND THE WIDE-BAND LIMIT

In the wide-band limit, where $\Gamma(\omega)$ is assumed constant everywhere, we find for the coupling coefficients the *finite*

[6]The replacement is motivated by the sign of the smallest eigenvalue of $\mathcal{M}^{\pm}_{\Delta E,\Delta E'}$ which is proportional to $\mathfrak{G}^2-\mathfrak{A}^2-\Delta G^2\leqslant 0$ where $\mathfrak{G}$ is the geometric mean, $\mathfrak{A}$ is the arithmetic mean of $\mathcal{F}^{\pm}_{\Delta E,T_{\mathrm{B}}}(t)$ and $\mathcal{F}^{\pm}_{\Delta E',T_{\mathrm{B}}}(t)$ (with $\mathfrak{G}^2\leqslant\mathfrak{A}^2$) and $\Delta G=[G_{\Delta E,T_{\mathrm{B}}}(t)-G_{\Delta E',T_{\mathrm{B}}}(t)]/2$, present in its off diagonals. Replacing $\mathfrak{A}$ with $\mathfrak{G}$ and setting $\Delta G=0$ in (A1) lifts the negative eigenvalue exactly to zero.

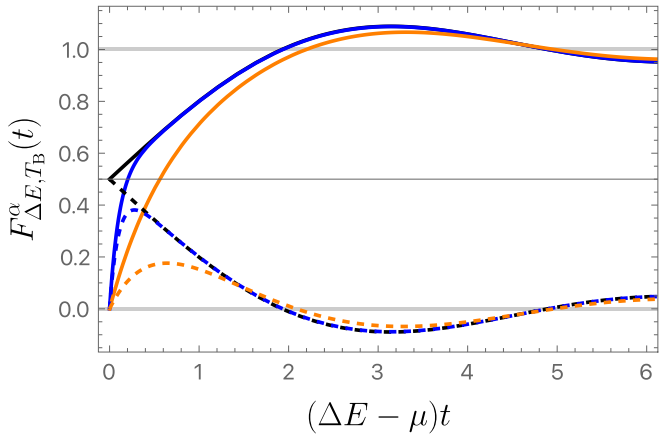

FIG. 7. Coefficients $F^{\alpha}_{\Delta E,T_B}(t)$ with $\alpha=-$ (solid lines) and $\alpha=+$ (dashed lines) as functions of time. The black lines show $F^{\alpha}_{\Delta E,T_B}(t)$ in the wide-band limit [cf. (17)] while other lines show $F^{\alpha}_{\Delta E,T_B}(t)$ for the Lorentzian (B1) with $\Delta_\Gamma=2(\Delta E-\mu)=2/\tau_c$ (orange) or $\Delta_\Gamma=10(\Delta E-\mu)=10/\tau_c$ (blue). The temperature is $T_B=0$ and $\Delta E-\mu>0$.

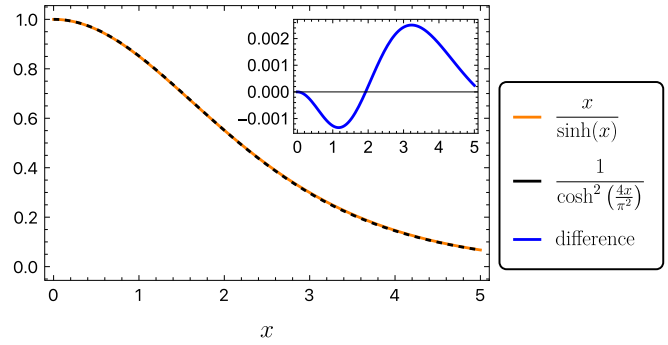

FIG. 8. Astonishing similarity between $x/\sinh(x)$ (orange) and $1/\cosh^2(4x/\pi^2)$ (black) with their difference in the inset (blue).

short-time limit $\lim_{t\to t_0} A^{\pm}_m(t,\Delta E)=\Gamma_m/2$. For any integrable function $\Gamma(\omega)$, however, the coefficients must vanish at short times $\lim_{t\to t_0} A^{\pm}_m(t,\Delta E)=0$ since $|A^{\pm}_m(t,\Delta E)|\leqslant \|\Gamma_m\|_1(t-t_0)/\pi$ with $\|\Gamma_m\|_1$ the L^1 norm. Consequently, Eqs. (16), (17), (28), and (29) cannot hold for very short times, $t-t_0\lesssim 1/\|\Gamma_m\|_1$. In the particular example of a Lorentz-type distribution

$$\Gamma_m(\omega)=\frac{\Gamma_m\Delta_\Gamma^2}{\Delta_\Gamma^2+(\Delta E-\omega)^2},\qquad \|\Gamma_m\|_1=\pi\,\Gamma_m\Delta_\Gamma \tag{B1}$$

the width Δ_Γ determines the scale of agreement with the wide-band limit, namely, for $t-t_0\gg 1/\Delta_\Gamma$ the coefficients $A^{\pm}_m(t,\Delta E)$ become well approximated by the wide-band limit (cf. Fig. 7). (For more general $\Gamma_m(\omega)$, the conditions hold analogously with Δ_Γ determined by the variation of $\Gamma(\omega)$ [27, Sec. 4].) If additionally $\Delta_\Gamma\gg 1/\tau_c=\max(k_BT_B,|\Delta E-\mu|)\gtrsim\Gamma_m$, the effects of the time-dependent temperature $T(t)$ become relevant.

APPENDIX C: DERIVATION OF THE $T(t)$ APPROXIMATION

In order to derive the approximation (23) we first need to introduce a useful similarity.

1. Functional similarity

There holds an astonishing similarity between the two hyperbolic functions

$$\frac{x}{\sinh(x)}\approx\frac{1}{\cosh^2(4x/\pi^2)}, \tag{C1}$$

as shown in Fig. 8. Despite intensive (re)search and discussion [58] we did not succeed in providing any elementary proof of it.[7] The constant $4/\pi^2$ is chosen by the requirement that both functions have equal integrals over $[0,\infty)$ which will have a physical significance in our applications.

2. Estimation of the integral (20)

Here, we will apply the discovered functional similarity (C1) to the integral (20). First we split the integrand into a product and use the similarity (C1) to obtain

$$I=T_B\int_0^{t-t_0}\frac{\sin(\Delta E'\tau)}{\sinh(\pi T_B\tau)}d\tau \tag{C2}$$

$$=\frac{\Delta E'}{\pi}\int_0^{t-t_0}\frac{\pi T_B\tau}{\sinh(\pi T_B\tau)}\frac{\sin(\Delta E'\tau)}{\Delta E'\tau}d\tau$$

$$\approx\frac{\Delta E'}{\pi}\int_0^{t-t_0}\frac{1}{\cosh^2(4T_B\tau/\pi)}\frac{\sin(\Delta E'\tau)}{\Delta E'\tau}d\tau \tag{C3}$$

with $\Delta E'\equiv\Delta E-\mu$ and omit the Boltzmann constant for shorter notation. In order to calculate this integral analytically, we use in the second factor the following trick: We observe that the first factor contributes significantly only for $4T_B\tau/\pi\lesssim 1$ (and is negligible otherwise) where the tanh function is almost linear so that we can replace $\tau\approx\pi\,\tanh(4T_B\tau/\pi)/(4T_B)$. This brings us to

$$I\approx\frac{\Delta E'}{\pi}\int_0^{t-t_0}\frac{1}{\cosh^2\left(\frac{4T_B\tau}{\pi}\right)}\frac{\sin\left(\frac{\pi\Delta E'}{4T_B}\tanh\left(\frac{4T_B\tau}{\pi}\right)\right)}{\frac{\pi\Delta E'}{4T_B}\tanh\left(\frac{4T_B\tau}{\pi}\right)}d\tau \tag{C4}$$

which, by substituting $u=\frac{\pi\Delta E'}{4T_B}\tanh(\frac{4T_B\tau}{\pi})$, leads to the result

$$I\approx\frac{1}{\pi}\mathrm{Si}\left[\frac{\pi\Delta E'}{4T_B}\tanh\left(\frac{4T_B(t-t_0)}{\pi}\right)\right], \tag{C5}$$

with Si being the sine integral function. The result inherits, however, the disadvantage of the exact coefficient $F_{\Delta E,T_B}(t)$ which overshoots beyond the allowed range, namely, $|I|$ increases above the value $\frac{1}{2}$ which leads to problems (cf. Sec. IV). But its behavior at early and late times t as well as small and large ΔE values is the same as in the tanh formula (23) which is free of that problem. Treating the excess oscillations (cf. Fig. 9) as an error of the first-order approximation

[7]The Taylor expansions of the reciprocals of both functions are very close to each other and grow exponentially fast. By this, both functions must decay exponentially and their absolute difference quickly gets negligibly small.

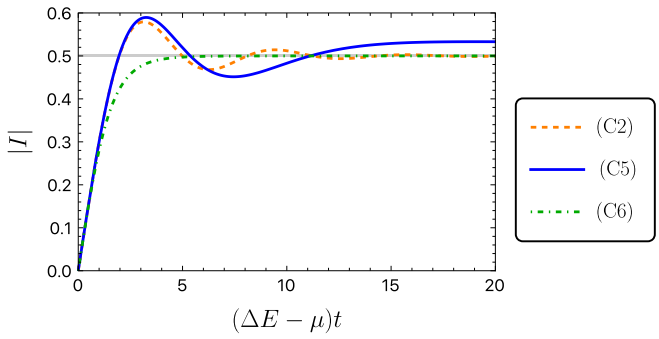

FIG. 9. Compared are the exact value of the integral I (C2) (orange), Si-tanh approximation (C5) (blue), and tanh-tanh approximation (C6) (green). The temperature of the bath is $k_B T_B = 0.08|\Delta E - \mu|$.

(in the coupling between the system and the bath) we want to correct it to physically acceptable range bearing physical interpretation. For this sake we observe that the sine integral (Si) function is close to $\mathrm{Si}(\pi x)/\pi \approx \tanh(2x)/2$ which builds the Fermi function and stays in the proper range (cf. Fig. 10). That replacement delivers the final approximation

$$I \approx \frac{1}{2}\tanh\left[\frac{\Delta E'}{2T_B}\tanh\left(\frac{4T_B(t-t_0)}{\pi}\right)\right] \tag{C6}$$

which, technically, presents our main result (23). The connection to the Fermi function is an essential point which allows us to interpret the final result, used in $F^{\pm}_{\Delta E,T_B}(t)$ (17), as the Fermi distribution with modified, time-dependent temperature $T(t)$ (25).

An alternative way to motivate this approximation [59, Chap. 3] (much simpler to derive but not uniform in ΔE) is to introduce the effective temperature by matching the slopes of the Fermi distribution and of the coefficient $F^{-}_{\Delta E,T_B}(t)$ at $\Delta E = \mu$

$$\frac{1}{4T(t)} = \left.\frac{\partial F^{-}_{\Delta E,T_B}(t)}{\partial \Delta E}\right|_{\Delta E=\mu} = \int_0^{t-t_0}\frac{T_B\tau\, d\tau}{\sinh(\pi T_B\tau)}. \tag{C7}$$

Using again the *astonishing similarity* $x/\sinh(x) \approx 1/\cosh^2(4x/\pi^2)$ [cf. (C1) in Appendix C 1], (25) follows.

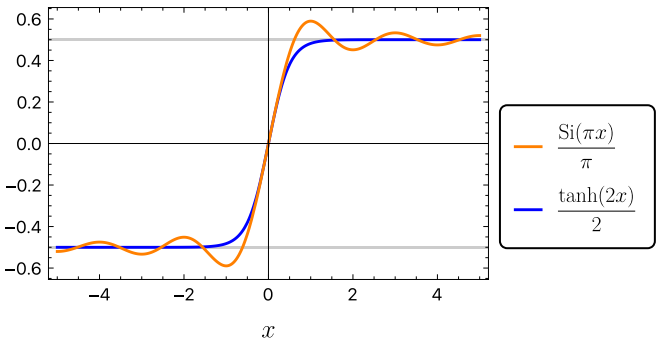

FIG. 10. Comparison of $\mathrm{Si}(\pi x)/\pi$ (orange) with $\tanh(2x)/2$ (blue) as functions of x. The maximal difference amounts ≈0.11 and vanishes for small and for large x.

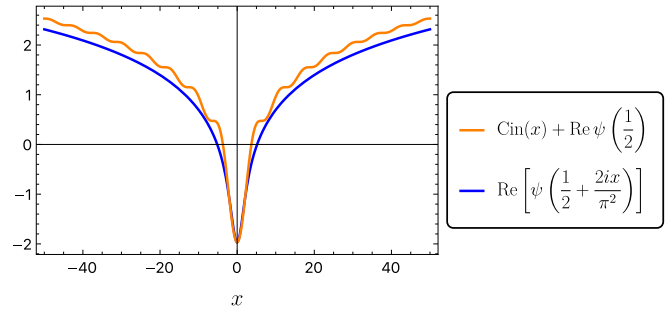

FIG. 11. Comparison of $\mathrm{Cin}(x) + \mathrm{Re}[\psi(1/2)]$ (orange) with $\mathrm{Re}[\psi(1/2 + 2ix/\pi^2)]$ (blue) as functions of x.

3. Estimation of the integral (29)

Applying the same approximations as discussed in Appendix C 2 to the integral (29), we derive

$$\begin{aligned} G_{\Delta E,T_B}(t) &= T_B\int_0^{t-t_0}\frac{1-\cos(\Delta E'\tau)}{\sinh(\pi T_B\tau)}d\tau \\ &\approx \frac{\Delta E'}{\pi}\int_0^{t-t_0}\frac{\pi T_B\tau}{\cosh^2(4T_B\tau/\pi)}\frac{1-\cos(\Delta E'\tau)}{\Delta E'\tau}d\tau \\ &\approx \frac{\Delta E'}{\pi}\int_0^{t-t_0}\frac{1}{\cosh^2\left(\frac{4T_B\tau}{\pi}\right)} \\ &\qquad\times\frac{1-\cos\left(\frac{\pi\Delta E'}{4T_B}\tanh\left(\frac{4T_B\tau}{\pi}\right)\right)}{\frac{\pi\Delta E'}{4T_B}\tanh\left(\frac{4T_B\tau}{\pi}\right)}d\tau \\ &= \frac{1}{\pi}\mathrm{Cin}\left[\frac{\pi\Delta E'}{4T_B}\tanh\left(\frac{4T_B(t-t_0)}{\pi}\right)\right] \end{aligned} \tag{C8}$$

with $\Delta E' \equiv \Delta E - \mu$ and omitting the Boltzmann constant for shorter notation. The cosine integral function is defined by

$$\mathrm{Cin}(x) = \int_0^x\frac{1-\cos(t)}{t}\mathrm{d}t \tag{C9}$$

and is close to $\mathrm{Cin}(x) \approx \mathrm{Re}[\psi(1/2 + 2ix/\pi^2) - \psi(1/2)]$ (cf. Fig. 11) where ψ is the digamma function [55, Sec. 6.3] which builds $G_{\Delta E,T_B}(\infty)$ [59, Ch. 3]. Using this replacement, we end up with the approximation

$$\begin{aligned} &G_{\Delta E,T_B}(t) \\ &\approx \frac{1}{\pi}\mathrm{Re}\left\{\psi\left[\frac{1}{2} + i\frac{\Delta E'}{2\pi T_B}\tanh\left(\frac{4T_B(t-t_0)}{\pi}\right)\right] - \psi\left(\frac{1}{2}\right)\right\} \end{aligned} \tag{C10}$$

which is identical to (31).

APPENDIX D: CORRELATIONS BETWEEN SYSTEM AND BATH

For the non-Coulomb interacting system described by (47), it is possible to give not only an exact expression of the quantum dot annihilation operator $c_H(t)$ [cf. (48)], but also an exact expression of the bath annihilation operators

$$b_{k,H}(t) = e^{-i\varepsilon_k t}b_k - i\,\overline{\gamma_k}\int_0^t c_H(s)e^{-i\varepsilon_k(t-s)}\mathrm{d}s, \tag{D1}$$

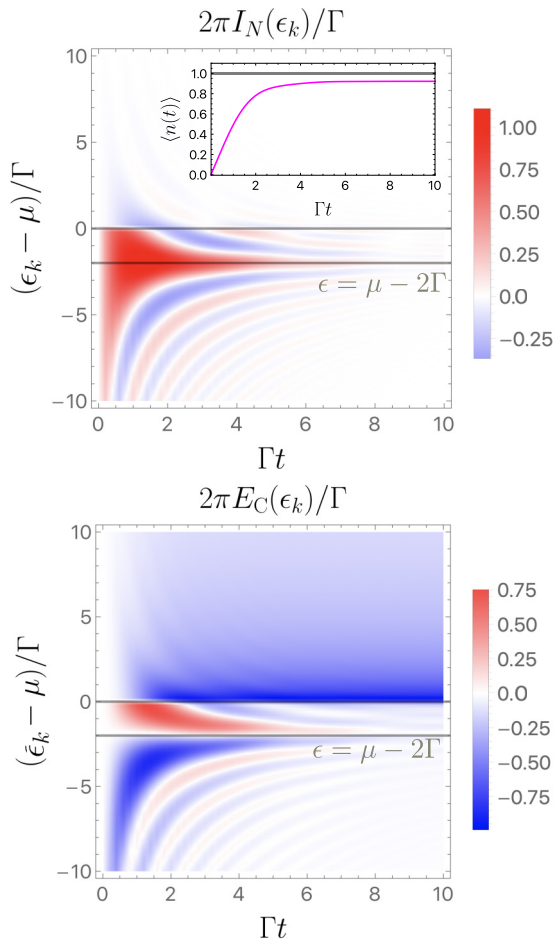

FIG. 12. Particle current $I(\varepsilon_k)$ (top) and the coupling energy $E_C(\varepsilon_k)$ (bottom) as functions of the energy of the bath modes ε_k and time t. The inset (top) shows the particle number of the system as a function of time. We consider a system given by the Hamiltonian (47) with the parameters $T_B = 0$ and $\varepsilon = \mu - 2\Gamma < \mu$ and an initially empty dot. The oscillations of off-resonant tunneling processes are given by $e^{i(\varepsilon_k-\varepsilon)t}$.

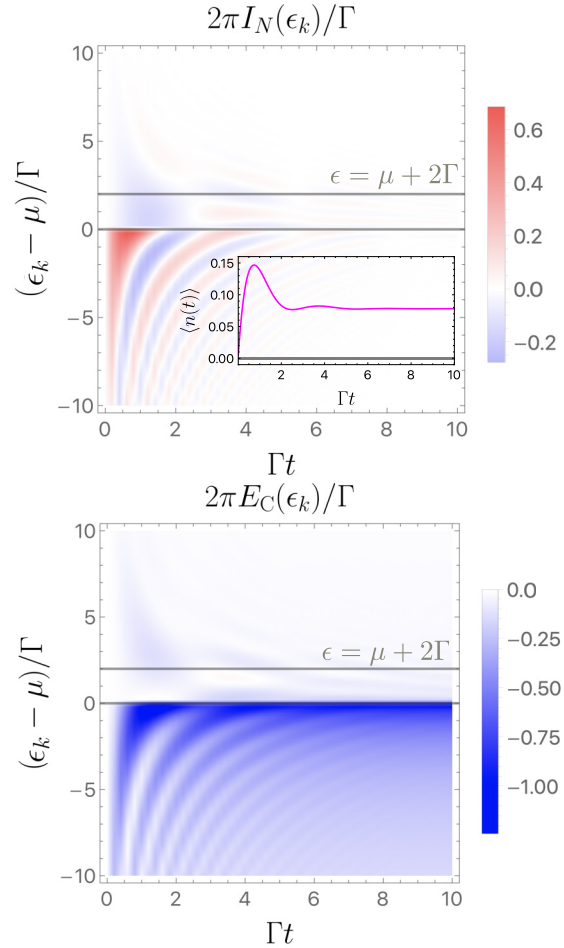

FIG. 13. Same as in Fig. 12 with the energy $\varepsilon = \mu + 2\Gamma > \mu$.

derived from the Heisenberg's equation of motion. This enables us to calculate the correlation $\langle c^\dagger b_k\rangle$ between the quantum dot and a bath mode with energy ε_k, of which the imaginary part gives the single-mode particle current

$$I_N(\varepsilon_k) = 2\,\mathrm{Im}[\gamma_k\langle c^\dagger b_k\rangle] \tag{D2}$$

from the bath mode k to the quantum dot. Summing $I_N(\varepsilon_k)$ over all modes k in the bath gives the total particle current satisfying the balance equation $\partial_t\langle c^\dagger c\rangle = \sum_k I(\varepsilon_k)$. The real part of the correlation corresponds to the single-mode coupling energy

$$E_C(\varepsilon_k) = 2\,\mathrm{Re}[\gamma_k\langle c^\dagger b_k\rangle] \tag{D3}$$

and the sum over all modes k in the bath gives the total coupling energy $\langle H_C\rangle = \sum_k E_C(\varepsilon_k)$.

Let us first consider an initial state different from the ground state of the quantum dot at $T_B = 0$ (in contrast to Fig. 5) in order to better see the relaxation process to the ground state. Let $\varepsilon < \mu$ and an initial particle number be $\langle n(0)\rangle = 0$. In Fig. 12, the quantities $I_N(\varepsilon_k)$ and $E_C(\varepsilon_k)$ are shown as functions of time and energy ε_k. From the conservation of energy for the quantum dot and bath alone, $H_S + H_B$, the current would flow only at the energy level $\varepsilon_k = \varepsilon$ but by including also the coupling energy H_C, the off-resonant currents at $\varepsilon_k \neq \varepsilon$ may appear. Bath electrons with $\varepsilon_k < \varepsilon$ reduce the coupling energy $E_C(\varepsilon_k)$ (cf. blue shading in Fig. 12, bottom) while electrons with $\varepsilon_k > \varepsilon$ increase the coupling energy $E_C(\varepsilon_k)$ (cf. red shading in Fig. 12, bottom) in time. These processes lead to relaxation towards the ground state of the quantum dot $\langle n\rangle = 1$ (cf. Fig. 12, inset), with a small deviation, $\langle n\rangle < 1$, caused by the off-resonant tunneling processes from the quantum dot back to bath states above the Fermi edge at $\varepsilon_k = \mu$. In order to satisfy the energy conservation, the coupling energies $E_C(\varepsilon_k)$ for $\varepsilon_k > \mu$ must become negative (cf. blue shading in Fig. 12, bottom). In consequence, the final state lies energetically higher than the ground state.

Finally, we consider a situation similar to the one shown in Fig. 5 with the quantum dot initially in its ground state $\langle n(0)\rangle = 0$ for $\varepsilon > \mu$. Here, the tunneling processes are not peaked around $\varepsilon_k \approx \varepsilon$ but around the Fermi level with off-resonant current from states below the Fermi level into the quantum dot (cf. red shading in Fig. 13, top). This also leads to an energy increase in the quantum dot that is compensated by the decrease of the coupling energies $E_C(\varepsilon_k)$ to negative values for states below the Fermi edge (cf. blue shading in Fig. 13, bottom).

[1] H.-P. Breuer and F. Petruccione, *The Theory of Open Quantum Systems* (Oxford University Press, Oxford, 2002).

[2] Y. Meir and N. S. Wingreen, Landauer formula for the current through an interacting electron region, Phys. Rev. Lett. **68**, 2512 (1992).

[3] A.-P. Jauho, N. S. Wingreen, and Y. Meir, Time-dependent transport in interacting and noninteracting resonant-tunneling systems, Phys. Rev. B **50**, 5528 (1994).

[4] R. Karrlein and H. Grabert, Exact time evolution and master equations for the damped harmonic oscillator, Phys. Rev. E **55**, 153 (1997).

[5] G. Stefanucci, Bound states in ab *initio* approaches to quantum transport: A time-dependent formulation, Phys. Rev. B **75**, 195115 (2007).

[6] P. Zedler, G. Schaller, G. Kiesslich, C. Emary, and T. Brandes, Weak-coupling approximations in non-Markovian transport, Phys. Rev. B **80**, 045309 (2009).

[7] W.-M. Zhang, P.-Y. Lo, H.-N. Xiong, M. W.-Y. Tu, and F. Nori, General non-Markovian dynamics of open quantum systems, Phys. Rev. Lett. **109**, 170402 (2012).

[8] G. E. Topp, T. Brandes, and G. Schaller, Steady-state thermodynamics of non-interacting transport beyond weak coupling, Europhys. Lett. **110**, 67003 (2015).

[9] M. M. Ali and W.-M. Zhang, Nonequilibrium transient dynamics of photon statistics, Phys. Rev. A **95**, 033830 (2017).

[10] E. Jussiau, M. Hasegawa, and R. S. Whitney, Signature of the transition to a bound state in thermoelectric quantum transport, Phys. Rev. B **100**, 115411 (2019).

[11] É. Jussiau and R. S. Whitney, Multiple perfectly transmitting states of a single level at strong coupling, Europhys. Lett. **129**, 47001 (2020).

[12] A. R. Kolovsky, Open Fermi-Hubbard model: Landauer's versus master equation approaches, Phys. Rev. B **102**, 174310 (2020).

[13] M. Nakagawa, N. Kawakami, and M. Ueda, Exact Liouvillian spectrum of a one-dimensional dissipative Hubbard model, Phys. Rev. Lett. **126**, 110404 (2021).

[14] F. Queisser and R. Schützhold, Environment-induced prerelaxation in the Mott-Hubbard model, Phys. Rev. B **99**, 155110 (2019).

[15] S. Nakajima, On quantum theory of transport phenomena: Steady diffusion, Prog. Theor. Phys. **20**, 948 (1958).

[16] R. Zwanzig, Ensemble method in the theory of irreversibility, J. Chem. Phys. **33**, 1338 (1960).

[17] J. König, J. Schmid, H. Schoeller, and G. Schön, Resonant tunneling through ultrasmall quantum dots: Zero-bias anomalies, magnetic-field dependence, and boson-assisted transport, Phys. Rev. B **54**, 16820 (1996).

[18] J. König, H. Schoeller, and G. Schön, Zero-bias anomalies and boson-assisted tunneling through quantum dots, Phys. Rev. Lett. **76**, 1715 (1996).

[19] C. Timm, Tunneling through molecules and quantum dots: Master-equation approaches, Phys. Rev. B **77**, 195416 (2008).

[20] X. Zhao, W. Shi, L.-A. Wu, and T. Yu, Fermionic stochastic Schrödinger equation and master equation: An open-system model, Phys. Rev. A **86**, 032116 (2012).

[21] A. G. Redfield, On the theory of relaxation processes, IBM J. Res. Dev. **1**, 19 (1957).

[22] R. Hartmann and W. T. Strunz, Accuracy assessment of perturbative master equations: Embracing nonpositivity, Phys. Rev. A **101**, 012103 (2020).

[23] R. Dümcke and H. Spohn, The proper form of the generator in the weak coupling limit, Z. Phys. B **34**, 419 (1979).

[24] A. Suárez, R. Silbey, and I. Oppenheim, Memory effects in the relaxation of quantum open systems, J. Chem. Phys. **97**, 5101 (1992).

[25] P. Gaspard and M. Nagaoka, Slippage of initial conditions for the Redfield master equation, J. Chem. Phys. **111**, 5668 (1999).

[26] E. Kleinherbers, N. Szpak, J. König, and R. Schützhold, Relaxation dynamics in a Hubbard dimer coupled to fermionic baths: Phenomenological description and its microscopic foundation, Phys. Rev. B **101**, 125131 (2020).

[27] L. Litzba, Relaxationsdynamik in Quantenpunktsystemen: Beschreibung durch zeitabhängige Lindblad-Operatoren und die Rolle von Kopplungsasymmetrie, Master's thesis, University Duisburg-Essen, 2022.

[28] E. B. Davies, Markovian master equations, Commun. Math. Phys. **39**, 91 (1974).

[29] G. Lindblad, On the generators of quantum dynamical semigroups, Commun. Math. Phys. **48**, 119 (1976).

[30] V. Gorini, A. Kossakowski, and E. C. G. Sudarshan, Completely positive dynamical semigroups of *N*-level systems, J. Math. Phys. **17**, 821 (1976).

[31] D. Chruściński and S. Pascazio, A brief history of the GKLS equation, Open Syst. Inf. Dynam. **24**, 1740001 (2017).

[32] J. O. González, L. A. Correa, G. Nocerino, J. P. Palao, D. Alonso, and G. Adesso, Testing the validity of the local and global GKLS master equations on an exactly solvable model, Open Syst. Inf. Dynam. **24**, 1740010 (2017).

[33] E. Kleinherbers, P. Stegmann, and J. König, Synchronized coherent charge oscillations in coupled double quantum dots, Phys. Rev. B **104**, 165304 (2021).

[34] N. Szpak, G. Schaller, R. Schützhold, and J. König, Relaxation to persistent currents in a Hubbard trimer coupled to fermionic baths, Phys. Rev. B **110**, 115131 (2024).

[35] H. Wichterich, M. J. Henrich, H.-P. Breuer, J. Gemmer, and M. Michel, Modeling heat transport through completely positive maps, Phys. Rev. E **76**, 031115 (2007).

[36] G. Kiršanskas, M. Franckié, and A. Wacker, Phenomenological position and energy resolving Lindblad approach to quantum kinetics, Phys. Rev. B **97**, 035432 (2018).

[37] D. Davidović, Completely positive, simple, and possibly highly accurate approximation of the Redfield equation, Quantum **4**, 326 (2020).

[38] F. Nathan and M. S. Rudner, Universal Lindblad equation for open quantum systems, Phys. Rev. B **102**, 115109 (2020).

[39] P. P. Potts, A. A. S. Kalaee, and A. Wacker, A thermodynamically consistent Markovian master equation beyond the secular approximation, New J. Phys. **23**, 123013 (2021).

[40] A. D'Abbruzzo, V. Cavina, and V. Giovannetti, A time-dependent regularization of the Redfield equation, SciPost Phys. **15**, 117 (2023).

[41] T. Becker, L.-N. Wu, and A. Eckardt, Lindbladian approximation beyond ultraweak coupling, Phys. Rev. E **104**, 014110 (2021).

[42] A. Trushechkin, Unified Gorini-Kossakowski-Lindblad-Sudarshan quantum master equation beyond the secular approximation, Phys. Rev. A **103**, 062226 (2021).

[43] R. S. Whitney, Staying positive: going beyond Lindblad with perturbative master equations, J. Phys. A: Math. Theor. **41**, 175304 (2008).

[44] G. Schaller, P. Zedler, and T. Brandes, Systematic perturbation theory for dynamical coarse-graining, Phys. Rev. A **79**, 032110 (2009).

[45] R. Dann, N. Megier, and R. Kosloff, Non-Markovian dynamics under time-translation symmetry, Phys. Rev. Res. **4**, 043075 (2022).

[46] K. Nestmann, V. Bruch, and M. R. Wegewijs, How quantum evolution with memory is generated in a time-local way, Phys. Rev. X **11**, 021041 (2021).

[47] L. Hebel and C. P. Slichter, Nuclear spin relaxation in normal and superconducting aluminum, Phys. Rev. **113**, 1504 (1959).

[48] A. Sher and H. Primakoff, Approach to equilibrium in quantal systems. II. Time-dependent temperatures and magnetic resonance, Phys. Rev. **130**, 1267 (1963).

[49] H. Andersen, I. Oppenheim, K. E. Shuler, and G. H. Weiss, Exact conditions for the preservation of a canonical distribution in Markovian relaxation processes, J. Math. Phys. **5**, 522 (1964).

[50] A. A. Budini, Quantum systems subject to the action of classical stochastic fields, Phys. Rev. A **64**, 052110 (2001).

[51] G. Schaller, C. Nietner, and T. Brandes, Relaxation dynamics of meso-reservoirs, New J. Phys. **16**, 125011 (2014).

[52] A. Riera-Campeny, A. Sanpera, and P. Strasberg, Open quantum systems coupled to finite baths: A hierarchy of master equations, Phys. Rev. E **105**, 054119 (2022).

[53] S. V. Moreira, P. Samuelsson, and P. P. Potts, Stochastic thermodynamics of a quantum dot coupled to a finite-size reservoir, Phys. Rev. Lett. **131**, 220405 (2023).

[54] G. Schaller, *Open Quantum Systems Far From Equilibrium*, (Springer, Berlin, 2014), Vol. 881.

[55] M. Abramowitz and I. A. Stegun, *Handbook of Mathematical Functions with Formulas, Graphs, and Mathematical tables*, (Dover, New York, 1968), Vol. 55.

[56] P. W. Anderson, Localized magnetic states in metals, Phys. Rev. **124**, 41 (1961).

[57] K. Nestmann and M. R. Wegewijs, Renormalization group for open quantum systems using environment temperature as flow parameter, SciPost Phys. **12**, 121 (2022).

[58] N. Szpak, Astonishing similarity of $x/\sinh(x)$ and $1/\cosh^2(4x/\pi^2)$, Mathematics Stack Exchange (2021), https://math.stackexchange.com/questions/4290199/astonishing-similarity-of-fracx-sinhx-and-frac1-cosh24x-pi2.

[59] E. Kleinherbers, Real-time analysis of single-electron transport through quantum dots, Ph.D. thesis, University Duisburg-Essen, 2022.